DOI:10.13476/j.cnki.nsbdqk.2021.0064
王盈心,李瑞杰,李玉婷.沙波形态对波浪要素的响应[J].南水北调与水利科技(中英文),2021,19(3):606-613,624. WANG Y X,LI R J,LI Y T. Response analysis of sand ripple form to wave elements[J]. South-to-North Water Transfers and Water Science & Technology,2021,19(3):606-613,624. (in Chinese)

沙波形态对波浪要素的响应

王盈心[1],李瑞杰[1,2],李玉婷[3]

(1.河海大学海岸灾害及防护教育部重点实验室,南京 210098;2.河海大学环境海洋实验室,南京 210098;
3.南京师范大学虚拟地理环境教育部重点实验室,南京 210023)

摘要:针对波浪作用下沙质底床上普遍存在的沙波现象,从沙波尺度角度出发,采用 1957—2018 年共 385 组野外实测资料和水槽试验资料进行拟合分析,得到基于近底波浪水质点运动强度的沙波波高、沙波波长计算公式。结果表明:与 Ni81 规则波、Ni81 不规则波、VR89 和 GK04 等 4 种典型模型对比,新的沙波波高和沙波波长计算公式具有更高的计算精度且表达形式上更具一般性;利用该沙波形态计算公式可改进床面粗糙度的计算方法,当应用于波浪底摩阻系数的求解时计算结果与实测数据较为吻合,即沙波形态对底边界层有效粗糙度的影响显著;新的沙波波高和沙波波长计算公式可较好地应用于波浪底摩阻系数的计算。

关键词:沙波运动;波浪;水流强度参数;有效粗糙度;波浪底摩阻

中图分类号:TV139.2 **文献标志码**:A **开放科学(资源服务)标志码(OSID)**:

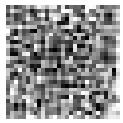

在波浪的作用下,近底局部扰动引起的近壁层流层产生波动使得泥沙颗粒起动,床面发生变形,形成广泛存在于冲击河流及海岸带处的沙波[1];同时,床面形态及沙波尺度影响波浪底边界层能量耗散与流动状态,不同的沙波尺度导致床面糙率发生明显变化,对底床总阻力产生不可忽略的影响,因此需要准确预测沙波形态发展规律。

针对沙波形态计算公式及其研究方法,国内外学者开展了大量研究。通过理论研究和数值模拟,证实波浪作用下水流运动与沙波状态存在相互作用[2-3],随着水流强度的增大,沙波逐渐形成并发展,沙波波高 η 和沙波波长 λ 随之增大并趋于平衡状态。同时沙波床面水流结构亦具有显著特征[4],张向东等[5]认为沙波二维几何特征与水流强度参数密切相关,床面波浪扰动影响沙波几何形状;Jin 等[6]依据水槽试验数据拟合得到近底波浪参数与沙波波长的数量关系;Soulsby 等[7]根据英国东部海岸沙波形态规律,提出波流共同作用下沙波波高和波长计算公式。

影响沙波尺度各要素的多样性和相互联系的复杂性,以及研究方法、资料来源与水域特征的差异,导致现有沙波形态特征的表达公式结构多样且在不同水力条件下的公式精度误差较大,计算公式缺少普遍性,为底床形状阻力的计算带来诸多不便。

本文从波浪条件与沙波形态相适应的角度出发,搜集近年来多组波浪作用下沙波形态的水槽试验和野外观测数据,采用数值拟合的方法建立沙波波高与波长一般形式表达式,分析水流强度参数对沙波形态的影响规律;通过探讨波浪作用下沙波床面粗糙度变化特征,提出考虑沙波尺度的有效粗糙度及波浪底摩阻系数的计算公式,为分析波浪作用下沙波床面形状阻力提供有效依据,为进一步研究床面总阻力及泥沙输运提供参考。

收稿日期:2020-11-30 **修回日期**:2021-03-16 **网络出版时间**:2021-03-26
网络出版地址:https://kns.cnki.net/kcms/detail/13.1430.TV.20210325.1906.002.html
基金项目:国家自然科学基金青年基金(51709091);中央级公益性科研院所基本科研业务费专项(HKY-JBYW-2020-03);江苏省自然科学基金青年基金(BK20170874)
作者简介:王盈心(1996—),女,天津人,主要从事河口海岸水动力学研究。E-mail:1115813500@qq.com
通信作者:李瑞杰(1963—),男,山东青岛人,博士生导师,主要从事物理海洋学、河口海岸物质输运研究。E-mail:rjli@hhu.edu.com.cn

1　现有沙波模型及试验数据集分析

1.1　现有沙波预测模型

在波浪条件下，沙波形态随着水流强度参数的变化而改变。作为反映波流共同作用的重要参数，水流强度参数表达式为

$$\Psi_w=u_w^2/(s-1)gd_{50} \tag{1}$$

式中：s 为泥沙相对密度，即泥沙密度与水体密度的比值 ρ_s/ρ；g 为重力加速度，m/s²；d_{50} 为泥沙中值粒径，m；u_w 为近底波浪水质点水平最大流速，m/s，根据微幅波理论 $u_w=\frac{2\pi A_w}{T\sinh kh}$，（$T$ 为波浪周期，s；h 为水深，m；A_w 为近底波浪水质点最大运动幅值，$A_w=u_wT/2\pi$，m），即 u_w 和 A_w 可由波浪参数计算。

研究表明，沙波波高、波长与 A_w 具有相同的数量级，当仅考虑自然波浪周期时，无量纲沙波波高和波长主要与 Ψ_w 相关。Nielsen[8]在已有数据的基础上，结合丹麦水利研究所的试验数据，将 η/A_w、λ/A_w与 Ψ_w 建立关系，提出基于规则波和不规则波两套独立的沙波尺度计算公式，分别是

对于试验水槽规则波（下文简称 Ni81 规则波）

$$\eta/A_w=0.275-0.022\Psi_w^{0.5} \tag{2}$$

$$\lambda/A_w=2.2-0.345\Psi_w^{0.34} \tag{3}$$

对于野外流场不规则波（Ni81 不规则波）

$$\eta/A_w=21\Psi_w^{-1.85} \tag{4}$$

$$\lambda/A_w=\exp[(693-0.37\ln^8\Psi_w)/(1\,000+0.75\ln^7\Psi_w)] \tag{5}$$

沙波形态与近底层水流稳定性有关，当水流强度超过泥沙的起动条件时，床面局部隆起并发展成沙波。Van[9]采用不规则波下测量的沙波数据，建立沙波尺度与 Ψ_w 的函数关系并将 Ψ_w 作为沙波尺度预测模型的判别依据（VR89）

$$\eta/A_w=\begin{cases}0.22 & \Psi_w\leqslant 10\\ 2.8\times10^{-13}(250-\Psi_w)^5 & 10<\Psi_w\leqslant 250\end{cases} \tag{6}$$

$$\eta/\lambda=\begin{cases}0.18 & \Psi_w\leqslant 10\\ 2.0\times10^{-7}(250-\Psi_w)^{2.5} & 10<\Psi_w\leqslant 250\end{cases} \tag{7}$$

通过精密仪器可以对近海海岸处的沙波尺度进行准确测量。Grasmeijer 等[10]根据荷兰海岸实测资料，对 Nielsen 模型修正，提出一种新的沙波尺度预测方法，用于描述不规则波下无量纲沙波高度和沙波陡度（GK04）

$$\eta/A_w=\begin{cases}0.275-0.022\Psi_w^{0.5} & \Psi_w<10\\ 2\Psi_w^{-1} & \Psi_w\geqslant 10\end{cases} \tag{8}$$

$$\eta/\lambda=\begin{cases}0.14 & \Psi_w<10\\ -0.078+0.355\Psi_w^{-0.221} & \Psi_w\geqslant 10\end{cases} \tag{9}$$

在 VR89 和 GK04 模型中，无量纲沙波波长能够通过沙波波高与陡度的比值求解，根据式（2）～（9），无量纲沙波波高和波长表达关系具备特征性，可归纳为一般形式表达式为

$$\eta/A_w=A\Psi_w^{\alpha}+B \tag{10}$$

$$\lambda/A_w=C\Psi_w^{\beta}+D \tag{11}$$

1.2　数据集与现有预测模型比较

为了比较上述沙波尺度经验公式的精度和适用性，将搜集的 1957—2018 年 385 组观测数据汇成数据集进行集成分析，研究沙波控制条件与沙波尺度的关系。数据类型包括 5 组野外流场勘测数据和 12 组水槽试验观测数据，波浪条件既有规则波也有不规则波，主要水动力参数和观测沙波波高、沙波波长范围见表 1。

表 1　数据集主要参数

Tab. 1　Main parameters of data set

数据来源	类型	h/m	H_r/m	T/s	d_{50}/mm	u_w/(m·s^{-1})	η/cm	λ/cm
Van Rijn(2007)[9]	野外	1.350～2.900	0.170～0.650	4.50～9.10	0.300	0.170～0.730	3.50～11.00	12.00～130.00
Grasmeijer 等(2004)[10]	野外	1.410～5.290	0.350～1.240	3.95～10.45	0.240	0.230～0.985	7.00～10.00	19.00～170.00
Williams 等(2004)[11]	水槽/野外	0.500～25.000	0.200～1.470	0.57～15.28	0.010～0.913	0.120～1.191	0～19.20	4.00～105.00
O'Donoghue 等(2001)[12]	水槽	0.400～0.750	0～19.000	2.00～15.00	0.180～0.440	0.209～0.940	0～19.36	6.00～121.00
Van der Werf 等(2006)[13]	水槽	0.750～0.800	0～35.000	3.10～12.50	0.210～0.440	0.447～0.775	1.50～14.10	14.40～110.70
Hanes 等(2001)[14]	野外	3.700～5.030	0.200～2.690	1.70～19.70	0.157	0.121～2.401	0.50～9.90	35.00～270.00
Thorne 等(2002)[15]	水槽			4.00～6.00	0.330	0.257～0.658	4.00～6.50	26.20～51.30
Faraci 等(2002)[16]	水槽	0.280～0.295	5.700～13.700	0.25～4.18	0.250	0.127～0.350	0.68～2.12	4.40～10.65
Pedocchi 等(2009)[17]	水槽			4.50～9.10	0.250	0.160～2.860	6.00～19.00	5.00～180.00
Yamaguchi 等(2011)[18]	水槽	0.200～0.600	0～0.222	1.25～5.00	0.320～0.730	0.158～0.407	0.70～4.10	4.70～25.70
Wang 等(2018)[19]	水槽			3.13～6.25	0.510	0.400～0.800	4.00～13.00	28.80～79.90
Petrotta 等(2018)[20]	水槽		0.057～0.157	0.95～1.10	0.250	0.241～0.521	0.44～1.49	3.34～6.14

表 1 中数据集所收录的已知水深 h 范围在 0.4～15.0 m;已知的有效波高 H_r 范围在 0～15.8 m;波浪周期 T 范围在 0.95～15.18 s,平均值 6.11 s;泥沙中值粒径 d_{50} 范围在 0.010 0～0.913 0 mm,平均粒径 0.188 5 mm;近底水质点运动最大流速 u_w 范围在 0.11～1.86 m/s,平均流速 0.55 m/s。根据已知水动力条件,按照研究者提出的沙波尺度预测模型求算沙波波高和沙波波长,对比分析预测值与实测值的吻合程度,判断预测模型的精度大小。

2　沙波尺度预测公式

沙波形态预测模型大多基于水槽试验数据及野外观测数据,受试验条件、观测地点和观测方法的局限性较大,往往缺乏普遍性。因此,建立一个新的沙波尺度预测模型,应用数据集尽可能地考虑到各种状态下沙波的发展规律,在现有公式的基础上提出一组精度更高、适用性更强的沙波尺度计算公式。

2.1　建立基于水流强度参数的沙波尺度预测模型

水流强度参数 Ψ_w 是反映近底边界层水动力特征的无量纲参数,将其作为模型变量能够很好地反映近底边界层水流条件,所以选择 Ψ_w 来描述无量纲沙波波高和沙波波长。当近底边界层流速较低时,底床形态较为规则,沙波波高和波长受泥沙粒径及近底波浪水质点最大运动幅值影响,η/A_w、λ/A_w 随 Ψ_w 变化不大,当水流强度增大时,沙波形态受 Ψ_w 的变化而显著改变,因此将 $\Psi_w \leqslant 10$ 和 $\Psi_w > 10$ 作为沙波波高和波长公式随近底波浪水质点水平最大流速递增的分段依据,在多组野外流场数据和水槽实测数据基础上拟合,提出平衡状态下连续性沙波波高、波长预测公式

$$\eta/A_w=\begin{cases}-0.001\,2\Psi_w^{1.8}+0.275 & \Psi_w\leqslant 10\\ 0.8\Psi_w^{-0.5}-0.05 & \Psi_w>10\end{cases} \tag{12}$$

$$\eta/A_w=\begin{cases}-0.057\Psi_w+1.92 & \Psi_w\leqslant 10\\ 4.5\Psi_w^{-0.2}-1.49 & \Psi_w>10\end{cases} \tag{13}$$

式中 Ψ_w 由式(1)计算。从式(12)和(13)的表达形式上看,当 $\Psi_w \leqslant 10$ 时,η/A_w 和 λ/A_w 变化不大,这与沙波尺度在底床水动力条件下的特征有关,Ni81 规则波模型、GK04 模型证实了这一点。由于在实际流场中波浪形态多变,存在风浪、涌浪及混合浪,Van[9]、Grasmeijer 等[10]的沙波形态研究是基于不规则波的,而在 Nielsen[8]研究中体现了规则波与不规则波的划分,于是将式(12)和(13)作为主要考虑自然波浪周期的沙波尺度预测公式。

2.2　新预测公式与经验模型对比

为探究公式(12)和(13)中水流强度参数的表达形式与沙波尺度的相关性,以 Ψ_w 为横坐标、η/A_w 和 λ/A_w 为纵坐标绘制关系曲线。将 Ni81 规则波、Ni81 不规则波、VR89 和 GK04 经验模型作为对照曲线,并通过数据集中沙波波高与波长的分布情况,检验式(12)和(13)与各预测模型的适用性。图 1 和 2 分别描述了 Ni81 规则波、Ni81 不规则波、VR89 模型、GK04 模型及式(12)和(13)计算值曲线。

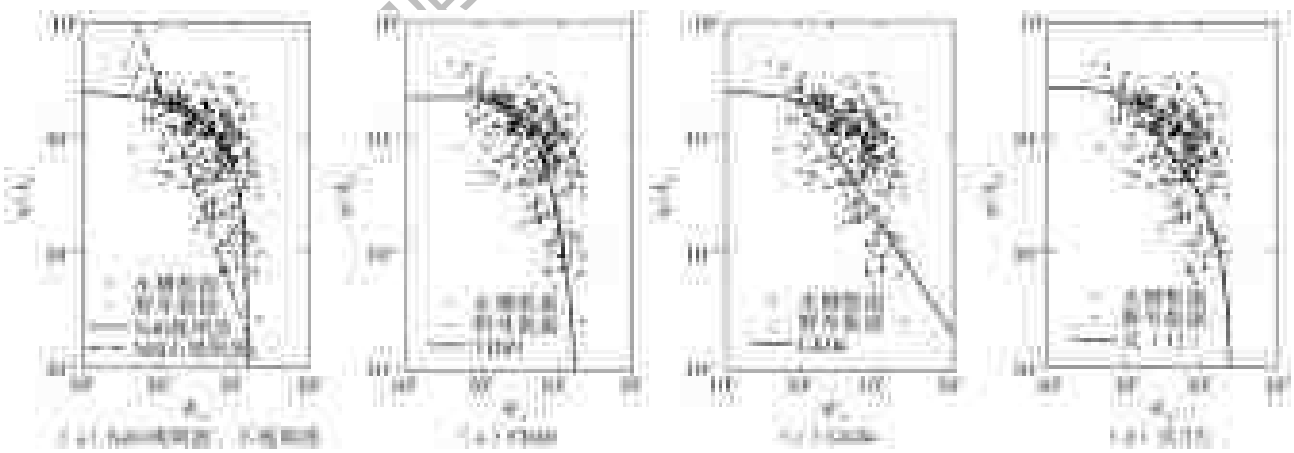

图 1　无量纲波高实测值与 Ni81 规则波、Ni81 不规则波、VR89 模型、GK04 模型及式(12)计算值曲线

Fig. 1　The measured value of dimensionless ripple height and the model of Ni81 regular wave, Ni81 irregular wave, VR89, GK04, and Eq. (12)

在一般情况下,床面附近的水流条件、床沙粒径与波浪条件三者对沙波尺度的变化起主要作用。推移质的运动强度直接取决于近底层水流流速,在水流作用下床面附近的泥沙颗粒发生起动使得床面变形,并逐步发展成典型的沙波。另外,床沙粒径同样影响沙波尺度的变化速率。Van[9]认为细沙颗粒在天然床层上的起动能力更强,容易形成规则形态沙波。除流速和泥沙粒径的影响外,沙波形态还受波浪参数影响,近底波轨振幅对沙波波高和波长的作用显著。图 1 体现了野外流场数据和水槽试验数据

沙波波高分布情况，相比于波长，波高的实测数据离散度较大且具有规律性分布，随水流强度的增大无量纲沙波波高实测值逐渐降低。根据计算曲线的特征，将 10 作为横坐标的分界点来分析：当 Ψ_w 值在 10 附近时，几种模型计算值变化幅度不大，随着水流强度的增加，无量纲沙波波高逐渐递减；当 $10<\Psi_w<250$ 时，η/A_w 值开始出现较大变化，部分值随水流强度的增加而减小，仍有一些波高值保持不变，这与沙波波高的变化速率有关。Ni81 规则波和 VR89 模型计算值为平滑的曲线，与实测资料更为吻合，而 Ni81 不规则波和 GK04 模型效果一般。Nielsen[8]认为不同状态波浪下沙波形态有所差异，因为规则波具有明显的波峰和波谷等显著二维特征，而不规则波多体现出三维特质，通过式(4)计算的 Ni81 不规则波偏差较大。总体上看，沙波波高的预测中 Ni81 规则波和 VR89 模型结果较好，而当较大时，计算结果偏差逐渐增大，对于野外流场中的沙波模型适用性一般；相较之下 VR89 模型对文献资料的计算值描述更好，同时适用于野外数据和水槽试验数据，GK04 模型在 $\Psi_w=10$ 处出现明显转折点，对沙波波高预测值整体偏低，尤其是对野外测量数据欠考虑。公式(12)作为野外数据和试验数据的经验拟合，对典型沙波波高公式做出校正，与其他模型相比适用性更好。

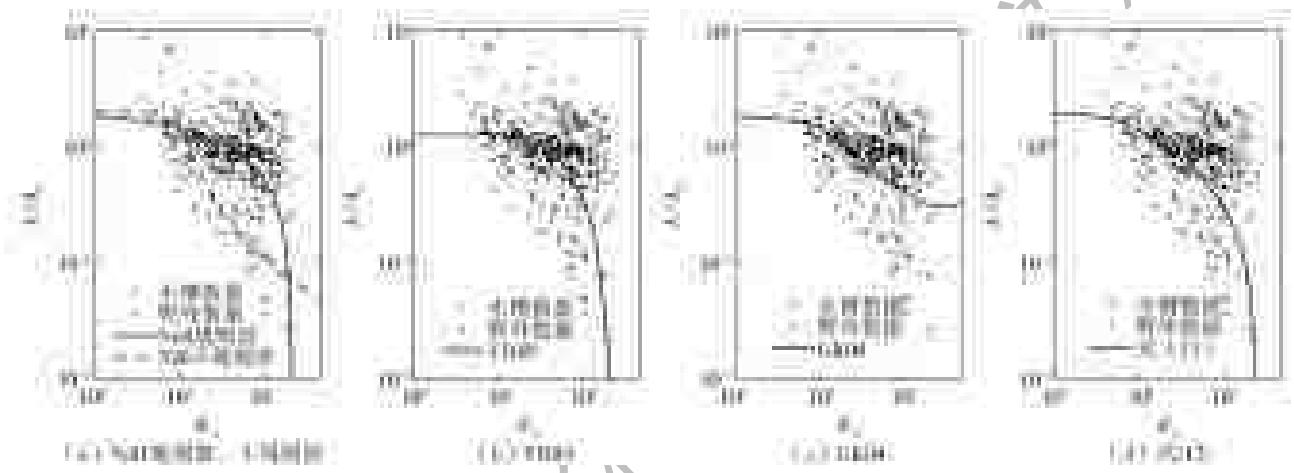

图 2　无量纲波长实测值与 Ni81 规则波、Ni81 不规则波、VR89 模型、GK04 模型及式(13)计算值曲线

Fig. 2　The measured value of dimensionless ripple length and the model of Ni81 regular wave, Ni81 irregular wave, VR89, GK04, and Eq. (13)

无量纲沙波波长的变化幅值比波高稍大，且分布较为集中，当 $10<\Psi_w<250$ 时，无量纲沙波波长的范围介于 0.01 至 10。从图 2 可知，实测数据在计算值附近波动较大，表明经验公式并不能完全准确地预测全尺度沙波的几何形状，正如 Grasmeijer 等[10]解释为波浪周期和泥沙粒径在近岸底床中较大且水槽槽宽一定程度上限制了沙波的发展，导致野外流场中波长明显较大而水槽试验中较小。在波流共同作用下，近底水质点波轨振幅持续存在，沙波一旦形成，沙波背后形成的旋涡就能够起到维持沙波的作用：当水流对沙波顶峰处的冲刷作用大于旋涡的维持作用时，沙波便不再保持稳定形态，通过许多试验证实无量纲沙波波长随 Ψ_w 增强而递减，如图 2 所示，沙波波长在水槽试验中的实测值具有下降的趋势，而在几组野外数据的变化体现不明显；当水流作用增加到足够大时，近底泥沙发生层移，沙波状态打破平衡，从逐渐发展直至衰减消亡，因此无量纲沙波波长将趋于 0，而不是趋于某值或增加，因此 Ni81 规则波和 VR89 模型曲线更为合理，GK04 模型在 Ψ_w 较大处的计算值不如前两者合理。几种典型沙波波长的计算方法各有利弊。Nielsen[8]对于沙波波长的计算与波高类似，Ni81 规则波与 Ni81 不规则波模型分别适用于野外流场和水槽试验，公式表达形式具有显著差异，在不规则波的结果计算中波高采用有效波高，然而式(5)表达形式较复杂，不便于使用；VR89 模型体现了更小的计算误差，且比 GK04 模型更优，但 VR89 模型需要通过 η/A_w 和 η/λ 的比值间接求解无量纲波长；Ni81 不规则波和 GK04 模型对于表 1 中数据的计算值存在偏差，Ni81 规则波和 VR89 模型实测值与计算值的比较效果略有改善，若不考虑野外数据，Ni81 不规则波和 GK04 模型对沙波波长的估算值仍然偏小。因此，式(13)在各模型的基础上进行拟合修正，得到 λ/A_w 的连续表达式。表 2 显示，沙波波长预测模型的误差高于沙波波高误差，表示各模型对沙波波高的预测普遍优于波长，RMSE 和 MAE 值在沙波波长中的计算结果偏高并不是由于模型预测能力有限，而是因为野外流场和水槽试验中沙波波长分布较为分散。

2.3　沙波形态公式精度验证

根据已知水动力条件,按照上述几种沙波尺度预测模型求算沙波波高和沙波波长,对比分析预测值与实测值的吻合程度,判断预测模型的精度大小。为比较公式精度,利用 2 种误差统计参数对沙波波高、沙波波长的预测值与实际值的符合程度进行评价,根据计算误差大小衡量公式的精度。

均方根误差 RMSE(root mean square error)是观测值与真值偏差的平方和与观测次数比值的平方根,也称回归系统的拟合标准差,用来衡量预测值 $x_{p,i}$ 同实测值 $x_{m,i}$ 之间的偏差,计算公式为

$$\Delta_{RMSE}=\sqrt{\frac{1}{N}\sum_{i=1}^{N}(x_{p,i}-x_{m,i})^2} \tag{14}$$

平均绝对误差 MAE(mean absolute error)能更好地反映预测值误差的实际情况,范围在[0,+∞),MAE 的值越小,说明预测模型拥有更好的精确度:当预测值与真实值完全吻合时 MAE 等于 0,即完美模型;误差越大,该值越大。计算公式为

$$\Delta_{MAE}=\frac{1}{N}\sum_{i=1}^{N}|x_{p,i}-x_{m,i}| \tag{15}$$

根据公式(14)和(15)得到预测模型计算误差,如表 2 所示,公式(12)和(13)计算的沙波波高和波长与各典型沙波模型相比,均方根误差和平均绝对误差更小,模型精度更高。

表 2　预测模型计算误差

Tab. 2　Prediction model calculation errors

模型	η		λ	
	MAE/cm	RMSE/cm	MAE/cm	RMSE/cm
Ni81	0.039 9	0.056 9	0.338 0	0.457 3
VR89	0.031 0	0.046 1	0.241 8	0.368 1
GK04	0.033 5	0.048 9	0.506 7	0.561 5
式(12)和(13)	0.028 1	0.040 4	0.223 4	0.333 0

3　沙波对波浪底摩阻系数的影响

3.1　沙波对床面粗糙度的作用

沙波的存在增加了床面的形状阻力,与平床相比,沙波床层上由沙波尺度引起的粗糙度变化更为显著。不少研究从沙波高度和沙波陡度来计算粗糙度公式,Kim 等[2]认为 $k_s\lambda/\eta^2$ 为常数。同样地,Nielsen 等[8]认为粗糙高度 k_s 与沙波尺寸成正比,即

$$k_s=\alpha\eta^2/\lambda \tag{16}$$

因此,可以通过比较 η^2/λ 值来确定水流中粗糙高度的作用。根据表 1 中数据集取值范围,假设 A_w 最大值与最小值分别取 3.00 m 和 0.05 m,η^2/λ 随 Ψ_w 的变化曲线见图 3。

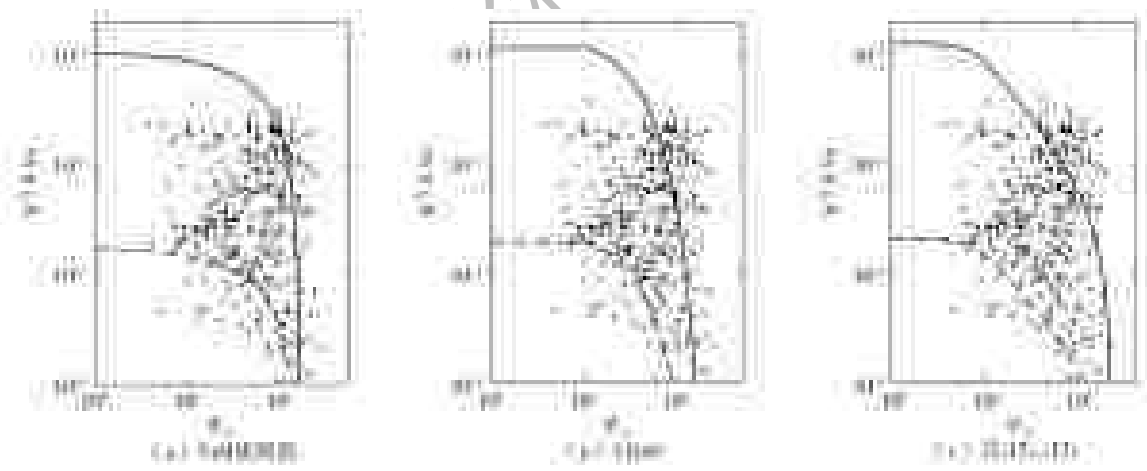

图 3　η^2/λ 实测值与 Ni81 规则波、VR89 模型及式(12)和(13)计算值曲线

Fig. 3　The measured value of η^2/λ and the model of Ni81 regular wave, VR89 and the calculated value curves of Eq. (12) and Eq. (13)

水槽试验中,不同的水槽断面可以观察到不同的沙波形态,表明沙波尺度与局部紊流结构相关。如图 3 所示,式(12)和(13)计算的 η^2/λ 值与 Ni81 规则波、VR89 模型的对比曲线证实此观点。随着水流强度的增加,床面粗糙高度逐渐递减直至为零,从 η^2/λ 值的变化速率上看,Ni81 规则波和 VR89 模型 η^2/λ 计算值曲线随 Ψ_w 的增大而减小,且急剧变陡,而式(12)和(13)的 η^2/λ 计算值曲线表示粗糙高度变化幅值先缓后陡。同时,根据实测数据的分布情况,Ni81 规则波、VR89 模型在水流强度较大时对沙波粗糙高度的计算较为局限,式(12)和(13)的 η^2/λ 计算曲线更加符合实测数据的分布规律,且更好地适用于多数野外实测数据。由于波浪的作用近底边界层产生床面切应力,在 Ψ_w 保持不变的情况下,A_w 值越大,η^2/λ 的变化幅度越为明显,这一观点在图 3 中有所体现。整体上 VR89 模型计算值略有偏低,而 Ni81 规则波的计算值对于波浪参数的变化不明显,相比于其他两种模型,式(12)和(13)对于

波浪参数的敏感性则更高，可以在更大程度上体现不同条件范围下粗糙度的变化趋势。

根据表1中多组野外数据和水槽实测数据，将实测沙波波高、沙波波长与通过计算或数值模拟[22]得到的阻力系数及粗糙高度对系数 α 进行率定，得到 $\alpha=24.5$。为验证式(12)和(13)中沙波波高和波长的计算方法与 α 取值的可靠性，同时探讨沙波形态对波浪要素的响应分析，在下一小节中将上述结论代入到波浪底摩阻系数的求算中，并通过实测数据进一步验证。

3.2　波浪作用下底摩阻系数的计算

当波浪进入浅水区后，床面对于波浪水流的摩擦阻力产生能量损失，特别是在坡度减缓的浅水海域，波浪底部摩阻损失较为显著。波浪作用下底床最大剪切力为

$$\tau_w=0.5\rho f_w u_w^2 \tag{17}$$

式中：ρ 为水体密度，g/cm^3；f_w 为波浪作用下底摩阻系数。层流及光滑紊流条件下的底摩阻系数主要由雷诺数决定，而粗糙紊流边界层底摩阻系数则与有效粗糙度 A_w/k_s 相关，f_w 与 A_w/k_s 之间存在关系式

$$\frac{1}{4\sqrt{f_w}}+\log\frac{1}{4\sqrt{f_w}}=\log\frac{A_w}{k_s}-0.08 \tag{18}$$

在平床状态下，粗糙高度 k_s 不受床面形态作用，与粒径大小相关；而在沙波床面的研究中考虑到床面形态特征对有效糙度的影响。因此，将式(16)作为考虑沙波存在的粗糙高度，为便于计算，在式(18)的基础上改进，采用显式表达式计算波浪摩阻系数[23]

$$f_w=\exp[5.213(A_w/k_s)^{-0.194}-5.977] \tag{19}$$

在 Davall 等[24]、Davies 等[25]近 20 年的研究中，粗糙度计算系数 α 取 8 至 30 不等。根据式(16)中 α 的率定结果，得到粗糙紊流下沙波形态有效粗糙度的计算公式为

$$\frac{A_w}{k_s}=\frac{A_w}{24.5\eta^2\lambda^{-1}} \tag{20}$$

其中，η 和 λ 由式(12)和(13)计算。将式(20)代入式(19)得到新的波浪底摩阻系数公式。采用文献[26-29]中的实测数据验证上式，其中 f_w 由文献数据直接给出或给定测量波浪边界层底部切应力，根据式(17)计算得到。由图4可看出波浪作用下底摩阻系数与有效粗糙度存在线性关系，曲线与实测数据吻合度较高，表明上述公式能够合理地计算波浪作用下的床面摩阻系数，同时表明沙波对于底层阻力有必然的影响，沙波尺度公式(12)和(13)可应用于波浪作用下粗糙紊流边界层床面底摩阻系数的计算。

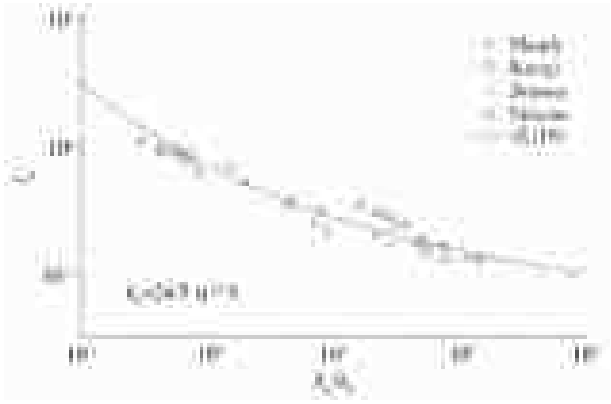

图4　波浪底摩阻系数与有效糙底的关系

Fig. 4　Relation between wave friction coefficient and effective roughness

4　结　论

(1)通过对比分析 Ni81 规则波、Ni81 不规则波、VR89 模型和 GK04 模型等几种典型沙波形态预测模型，提出一组新的沙波波高和沙波波长计算公式，该公式为表达形式更具一般性，便于工程应用。

(2)无量纲沙波波高和波长与水流强度参数存在相关关系，随水流强度参数的增大逐渐减小，通过与几种现有模型对比分析，式(12)和(13)可以更好地描述沙波形态变化规律，在实测资料的验证下新的沙波形态计算公式具有较高的计算精度。

(3)将沙波波高和沙波波长计算公式应用到底床粗糙度的计算中，对比现有成果，式(12)和(13)能够较好地体现沙波形态对粗糙度的影响，对波浪参数具有较高的敏感性。根据实测值对粗糙度公式中的参数进行率定，取 $\alpha=24.5$。将粗糙度计算公式与沙波尺度计算公式应用到波浪作用下底摩阻系数的计算中，在试验数据的验证下底摩阻系数预测曲线与实际值吻合较好，表明公式具有较高的适用性。

参考文献(References)：

[1] 肖千璐，李瑞杰，王梅菊. 波浪作用下沙纹床面形态及底摩阻系数研究[J]. 水运工程，2017(5)：12-18. (XIAO Q L，LI R J，WANG M J. Study on wave-induced ripple characteristics and bottom friction factors[J]. Port & Waterway Engineering，2017(5)：12-18. (in Chinese)) DOI：10.3969/j.issn.1002-4972.2017.05.003.

[2] 戴文鸿，苗伟波，高嵩，等. 弯道水流运动及床面变形数值模拟研究进展[J]. 南水北调与水利科技，2014，12(3)：121-126. (DAI W H，MIAO W B，GAO S，et al. Development of study on numerical simulation of meandering river flow and bed deformation[J]. South-to-North Water Transfers and Water Science & Technology，2014，12(3)：121-126. (in Chinese)) DOI：10.

13476/j. cnki. nsbdqk. 2014. 03. 027.

[3] WANG L, CUTHBERTSON A, PENDER G. Bed load sediment transport and morphological evolution in a degrading uniform sediment channel under unsteady flow hydrographs [J]. Water Resources Research, 2019, 55(7): 5431-5452. DOI: 10. 1029/2018WR024413.

[4] 马殿光, 董伟良, 徐俊锋. 沙波迎流面流速分布公式[J]. 水科学进展, 2015, 26(3): 396-403. (MA D G, DONG W L, XU J F. Velocity distribution of nonuniform flow on the stoss side over dunes[J]. Advances in Water Science, 2015, 26(3): 396-403. (in Chinese)) DOI: 10. 14042/j. cnki. 32. 1309. 2015. 02. 017.

[5] 张向东, 唐立模, 杨军, 等. 沙纹形态特征与水流强度的关系研究[J]. 人民长江, 2013, 44(5): 61-65. (ZHANG X D, TANG L M, YANG J, et al. Study of relationship between geometry characteristics of sand ripple and flow intensity[J]. Yangtze River, 2013, 44(5): 61-65. (in Chinese)) DOI: 10. 3969/j. issn. 1001-4179. 2013. 05. 016.

[6] JIN C, COCO G, TINOCO R O. Laboratory experiments on the role of hysteresis, defect dynamics and initial perturbation on wave-generated ripple development [J]. Coastal and Shelf Science, 2019, 224: 142-153. DOI: 10. 1016/j. ecss. 2019. 05. 003.

[7] SOULSBY R L, WHITEHOUSE R J S, MARTEN K V. Prediction of time-evolving sand ripples in shelf seas [J]. Continental Shelf Research, 2012, 38: 47-62. DOI: 10. 1016/j. csr. 2012. 02. 016.

[8] NIELSEN P. Dynamics and geometry of wave-generated ripples [J]. Journal of Geophysical Research: Oceans, 1981, 86(C7): 6467-6472. DOI: 10. 1029/JC086iC07p06467.

[9] VAN R L C. Unified view of sediment transport by currents and waves. I: Initiation of motion, bed roughness, and bed-load transport[J]. Journal of Hydraulic Engineering, 2007, 133(6): 649-667. DOI: 10. 1061/(ASCE)0733-9429(2007)133: 6(649).

[10] GRASMEIJER B T, KLEINHANS M G. Observed and predicted bed forms and their effect on suspended sand concentrations[J]. Coastal Engineering, 2004, 51(5/6): 351-371. DOI: 10. 1016/j. coastaleng. 2004. 05. 001.

[11] WILLIAMS J J, BELL P S, THORNE P D, et al. Measurement and prediction of wave-generated suborbital ripples[J]. Journal of Geophysical Research: Oceans, 2004, 109(C2): 1-18. DOI: 10. 1029/2003JC001882.

[12] O'DONOGHUE T, CLUBB G S. Sand ripples generated by regular oscillatory flow[J]. Coastal Engineering, 2001, 44(2): 101-115. DOI: 10. 1016/S0378-3839(01)00025-4.

[13] VAN D W, RIBBERINK J S, O'DONOGHUE T, et al. Modelling and measurement of sand transport processes over full-scale ripples in oscillatory flow [J]. Coastal Engineering, 2006, 53(8): 657-673. DOI: 10. 1016/j. coastaleng. 2006. 02. 002.

[14] HANES D M, ALYMOV V, CHANG Y S, et al. Wave-formed sand ripples at Duck, north Carolina [J]. Journal of Geophysical Research: Oceans, 2001, 106(C10): 22575-22592. DOI: 10. 1029/2000JC000337.

[15] THORNE P D. Suspended sediments under waves measured in a large-scale flume facility[J]. Journal of Geophysical Research, 2002, 107(C8): 4-1-4-16. DOI: 10. 1029/2001JC000988.

[16] FARACI C, FOTI E. Geometry, migration and evolution of small-scale bedforms generated by regular and irregular waves [J]. Coastal Engineering, 2002, 47(1): 35-52. DOI: 10. 1016/S0378-3839(02)00097-2.

[17] PEDOCCHI F, GARCÍA M H. Ripple morphology under oscillatory flow: 2. Experiments[J]. Journal of Geophysical Research, 2009, 114(C12): 1-17. DOI: 10. 1029/2009JC005356.

[18] YAMAGUCHI N, SEKIGUCHI H. Variability of wave-induced ripple migration in wave-flume experiments and its implications for sediment transport[J]. Coastal Engineering, 2011, 58(8): 671-677. DOI: 10. 1016/j. coastaleng. 2011. 03. 001.

[19] WANG D, YUAN J. Bottom-slope-induced net sediment transport rate under oscillatory flows in the rippled-bed regime [J]. Journal of Geophysical Research: Oceans, 2018, 123(10): 7308-7331. DOI: 10. 1029/2018JC013810.

[20] PETROTTA C, FARACI C, PIETRO S, et al. Experimental investigation on sea ripple evolution over sloping beaches [J]. Ocean Dynamics, 2018, 68: 1221-1237. DOI: 10. 1007/s10236-018-1197-x.

[21] KIM H, BAEK S W, HWANG D H, et al. Intra-wave-phase cross-shore profile modelling by using boundary-fitted slowly moving grid[J]. Mathematical Models in Engineering, 2016, 2(2): 78-93. DOI: 10. 21595/mme. 2016. 16641.

[22] 戴路, 李瑞杰, 丰青, 等. 一般形式的阻力系数公式及其在挟沙力计算中的应用[J]. 泥沙研究, 2016(2), 7-13. (DAI L, LI R J, FENG Q, et al. A general formula of resistance coefficient and its application in sediment-carrying capacity computation [J]. Journal of Sediment Research, 2016(2), 7-13. (in Chinese)) DOI: 10. 16239/j. cnki. 0468-155x. 2016. 02. 002.

[23] RODRÍGUEZ-ABUDO S, FOSTER D L. Direct esti-

mates of friction factors for a mobile rippled bed[J]. Journal of Geophysical Research: Oceans, 2017, 122(1): 80-92. 10.1002/2016JC012055.

[24] DUVALL M S, WIBERG P L, KIRWAN M L. Controls on sediment suspension, flux, and marsh deposition near a bay-marsh boundary[J]. Estuaries and Coasts, 2019, 42(2): 403-424. DOI: 10.1007/s12237-018-0478-4

[25] DAVIES A G, THORNE P D. On the suspension of graded sediment by waves above ripples: Inferences of convective and diffusive processes[J]. Continental Shelf Research, 2016, 112(1), 46-67. DOI: 10.1016/j.csr.2015.10.006.

[26] JOHN F A, SLEATH S. Wallbridge. pickup from rippled beds in oscillatory flow[J]. Journal of Waterway Port Coastal and Ocean Engineering, 2002, 126(6): 228-237. DOI: 10.1061/(asce)0733-950x(2002)128: 6(228).

[27] SIMPSON D E, KEMP P H. Quality and quantity of stormwater runoff from a commercial land-use catchment in Natal, South Africa[J]. Water Science & Technology, 2015, 14(4/5): 323-338. DOI: 10.2166/wst.1982.0110.

[28] JENSEN B L, SUMER B M, FREDSE J. Turbulent oscillatory boundary layers at high Reynolds numbers [J]. Journal of Fluid Mechanics, 2006, 206(4): 265-297. DOI: 10.1017/S0022112089002302.

[29] AHMADIAN A S, SIMONS R R. Estimation of nearshore wave transmission for submerged breakwaters using a data-driven predictive model[J]. Neural Computing and Applications, 2018, 29(10): 705-719. DOI: 10.1007/s00521-016-2587-y.

Response analysis of sand ripple form to wave elements

WANG Yingxin[1], LI Ruijie[1,2], LI Yuting[3]

(1. *Key Laboratory of Coastal Disaster and Defence, Ministry of Education, Hohai University, Nanjing* 210098, *China*; 2. *Laboratory of Ocean Environment, Hohai University, Nanjing* 210098, *China*; 3. *Key Laboratory of Virtual Geographic Environment of Ministry of Education, Nanjing Normal University, Nanjing* 210023, *China*)

Abstract: Sand ripple movement widely exists in the impinged river and coastal zone, and the ripple shape leads to the obvious change of bed surface roughness, which has a significant influence on the total resistance of the bottom bed. For ripple height and ripple length calculation methods, many scholars did comprehensive research, but due to the diversity of each factor affect the ripple scale and the complexity of interconnected, the different research methods, and the differences between the source and water features, lead to the existing formula of ripple shape structure that is diversiform, and the calculation formula lack universality due to an error in the formula under different hydraulic conditions.

The general expression for calculating ripple height and ripple length was established based on adapting wave conditions to ripple shape. A total of 385 groups of field measured data and flume experimental data were used for fitting analysis from 1957 to 2018, and the calculation formula for ripple height and ripple length based on the mobility number of near-bottom wave water quality point was obtained. Compared with the existing ripple calculation models, the influence rules of the mobility number on the ripple shape and the advantages and disadvantages of each model were analyzed and demonstrated. Two statistical error parameters RMSE and MAE were used to evaluate the degree of concordance between the predicted ripple height and ripple length of each prediction model and the actual value, and the accuracy of the formula was measured according to the calculation error. At the same time, the calculation formulas of ripple height and ripple length were applied to calculate the bottom rough height of the bed. The variation characteristics of ripple surface roughness under wave action and the rationality of the ripple formula were discussed by comparing with the existing models, and the parameters in the formula were calibrated using measured data. The formula of ripple shape and bottom roughness were introduced into the calculation of the bottom friction coefficient of waves, and the influence of the calculation method on the calculation result of the bottom friction coefficient was discussed.

The Eq. (12) and Eq. (13) for the ripple height and the ripple length were obtained by fitting analysis of measured data. The analysis showed that the dimensionless ripple height and ripple length were related to the mobility number, and decrease with the increase of the mobility number. Based on measured data, compared with Ni81 regular wave model, Ni81 irregular wave model, VR89 model, and GK04 model, the calculated values of Eq. (12) and Eq. (13) had higher accuracy, which could be applied to the prediction of the ripple height and the ripple length in both field flow and flume experiment, and the expression form of the formula was more general. The bottom roughness had a high sensitivity to wave parameters. According to the measured value, the parameter α in the bottom roughness formula was calibrated, and α was set as 24.5. The ripple scale formula was substituted into the bottom friction coefficient under wave action, and the calculated results were in good agreement with the representative experimental data, indicating that the newly obtained ripple scale formula could be applied for bottom friction coefficient calculation.

（下转第 624 页）

control levee considering ecological resilience of riparian zone, so as to provide decision support for the formulation of urban levee safety optimization scheme in the context of climate change.

Aiming at the uncertainty in the elevation optimization model of flood control levee, an interval mixed-integer stochastic robust optimization model was established. The model could not only regulate the ecological resilience of riparian zone to resist flood, but also deal with the uncertainty of parameters in the optimal design of levee elevation. These uncertain parameters included the flood peak level in the form of the probability distribution function and the economic cost in the form of interval value. Besides, considering the dynamic change of riparian ecosystem resilience to flood due to the impact of climate change, binary variables were introduced into the model to indicate whether the restoration and reconstruction of the ecological riparian zone were necessary. Moreover, decision-makers could also make a quantitative trade-off between system stability and economy by setting different risk parameters.

The developed model was applied to three planned areas located on both sides of the urban river. Under the condition of the different flood peak levels and riparian ecological resilience, the optimal design elevation of the flood control levee was obtained. The result showed that when the value of the risk parameter was 0.5, the system cost was [4.872, 6.552] million yuan. Before ecological reconstruction, the designed elevations of the flood control levees in the three areas were 11.8, [13.0, 13.8], 13.9 meters, respectively. It could be seen that the impact of uncertain factors caused by climate change on the second region was more obvious. Affected by extreme flood disasters, ecological reconstruction was needed in the first area to increase the resilience of the riparian zone against floods when the flood level ranges from medium-high to very-high. Correspondingly, the levee needed to be raised [2.8, 3.5], [3.5, 4.0], and [2.8, 3.5] meters respectively. The situation in the second area seemed to be different. It only carried out ecological reconstruction at very-high flood level, and after the reconstruction, the flood-control levee in this area increased [3.0, 4.0] meters. In addition, when the flood level was medium, high, and very-high, the flood overflowed the levee and submerged the third area. Furthermore, when the value of the risk parameter increased from 0 to 1, the system cost increased from [4.809, 6.437] million yuan to [4.926, 6.656] million yuan. At the same time, the stability of the model result was improved.

It could be seen from the results that when the overall flood control capacity of the region was not enough to resist the intrusion of the extreme flood, the model would prioritize the allocation of excessive flood to subareas where the cost of flood damage was lower. Also, it must be recognized that there was a trade-off between system stability and economy. Therefore, in practical application, decision-makers should comprehensively consider the extreme flood risk caused by climate change and the system's resilience to resist extreme floods. Based on this, appropriate risk parameter values should be selected to control the proportionality of the optimization results, so as to obtain a better decision-making scheme. The results of the case showed that the model could provide decision-makers with a reasonable flood control optimization strategy that considered the ecological resilience of riparian zones, and could provide a reference for the study of urban levee safety strategy under climate change.

Key words: ecological resilience; riparian zone; flood levee; uncertainty; op timization model

(上接第 613 页)

The shape of the bed surface and the ripple scale affect the energy dissipation and flow state of the wave bottom boundary layer, and the ripple scale had a significant effect on the roughness of the bed surface. However, there were some differences in the calculation methods of the ripple height and the ripple length. The new formula for calculating the shape of the ripple was more accurate and could better reflect the influence of the ripple scale on the friction coefficient of wave bottom. The new formula is more general in expression form and easy to be applied in engineering. This paper provides an effective basis for analyzing the shape resistance of bed surface under wave action and also provides a reference for further studying the total resistance of bed surface and sediment transport.

Key words: sand ripple moving; wave; mobility number; effective roughness; wave friction